XVIII International Conference on Water Resources
CMWR 2010
J. Carrera (Ed)

PALEOCLIMATE ANALYSES OF DENSITY-DEPENDENT GROUNDWATER FLOW WITH PSEUDO-PERMAFROST IN DISCRETELY FRACTURED CRYSTALLINE ROCK SETTINGS

Stefano D. Normani and Jonathan F. Sykes

Department of Civil and Environmental Engineering
University of Waterloo, Waterloo, Ontario, Canada, N2L 3G1
e-mail: sdnorman@uwaterloo.ca, web page: http://www.civil.uwaterloo.ca

Key words: paleoclimate, Canadian Shield, hydromechanical, ice-sheet, glacial meltwater

Summary. A high resolution sub-regional scale ($104\,km^2$) density-dependent, groundwater flow model with fracture zone networks, hydromechanical coupling and pseudo-permafrost, was developed from a larger $5734\,km^2$ regional scale groundwater flow model of a Canadian Shield setting in fractured crystalline rock. The objective of the work is to examine the impact of glaciation and deglaciation on aspects of regional and sub-regional groundwater flow that are relevant to the long-term performance of a hypothetical nuclear fuel repository. The discrete fracture dual continuum numerical model FRAC3DVS-OPG was used for all simulations. A discrete fracture zone network model delineated from surface features was superimposed onto an 789887 element flow domain mesh. Orthogonal fracture faces (between adjacent finite element grid blocks) were used to best represent the irregular discrete fracture zone network. The crystalline rock between these structural discontinuities was assigned hydraulic and mechanical properties characteristic of those reported for the Canadian Shield at the Underground Research Laboratory at Pinawa, Manitoba.

The multiple 121000 year North American continental scale paleoclimate simulations are provided by W.R. Peltier using the University of Toronto Glacial Systems Model, whereby values of ice sheet normal stress, and proglacial lake depth are applied to the sub-regional model as surface boundary conditions. Thermal conditions resulting in permafrost formation are applied as a permeability reduction to both three-dimensional grid blocks and fractures that lie within the time varying permafrost zone. Density-dependent flow is required due to the presence of pore fluids deep in the Canadian Shield with densities of up to $1200\,kg/m^3$ and total dissolved solids concentrations in excess of $300\,g/L$. Hydromechanical coupling between the rock matrix and the pore fluid, due to the ice sheet normal stress, is included in the simulations. The flow model includes vertical strain and assumes that areal loads are homogeneous. The importance of hydromechanical coupling is shown using the sub-regional model to investigate the effect on the depth of glacial meltwater migration into the subsurface.

1 INTRODUCTION

Over the past 900000 years, the Canadian Shield has experienced approximately 9 episodes of complete glaciation. During the glaciation cycles, the entire Canadian land mass has been covered by a series of continental ice-sheets whose maximum thickness reached 4 km.[1]

Climate change and glaciation are not only a concern for the Canadian nuclear fuel waste disposal concept, but also for the Swedish[2,3] and Finnish concepts.[4] Peltier[1] and Marshall et al.[5] have developed glaciological reconstructions of the Laurentide Ice-Sheet using numerical models. During ice-sheet advance, a repository site would evolve from periglacial to subglacial with the site eventually overlain by up to 4 km of ice. Permafrost several hundred metres thick develops in advance of the ice-sheet.[1]

2 HYDROMECHANICAL COUPLING

One-dimensional vertical loading and unloading due to glaciation, erosion, or deposition, is a common simplification that can be applied in hydromechanical coupling; this coupling is applied to porous media, ignoring mechanical effects on fractures.[6,7,8] Assuming that the porous media, solid grains, and pore fluid are all compressible, the specific storage S_s is defined as:

$$S_s = \rho\, g \left[\left(\frac{1}{K} - \frac{1}{K_s} \right) (1-\lambda) + n \left(\frac{1}{K_f} - \frac{1}{K_s} \right) \right], \quad \lambda = \frac{2\alpha(1-2\nu)}{3(1-\nu)}, \quad \alpha = 1 - \frac{K}{K_s} \tag{1}$$

where ρ is the fluid density [M/L^3]; g is the gravitational constant [L/T^2]; K is the drained bulk modulus of the porous media [M/T^{2}L]; K_s is the bulk modulus of the solids in the porous media [M/T^{2}L]; K_f is the bulk modulus of the pore fluid [M/T^{2}L]; α is the Biot coefficient [/]; and ν is the Poisson's ratio [/]. The bulk modulus K is defined as the reciprocal of compressibility, therefore $K = 1/\beta$ as presented in Jaeger et al.[8]

The effect of mechanically loading the surface of a porous media is to transfer the load to both the porous media, and the pore fluid; the effects of mechanical loading and pore pressure affect each other, and are thus coupled. The groundwater flow equation can be modified to account for one-dimensional hydromechanical coupling as follows:

$$\frac{\partial}{\partial x_i} \left[K_{ij} \left(\frac{\partial h}{\partial x_j} + \rho_r \frac{\partial z}{\partial x_j} \right) \right] \pm Q = S_s \frac{\partial h}{\partial t} - \frac{S_s\, \zeta}{\rho\, g} \frac{\partial \sigma_{zz}}{\partial t} \qquad i, j = 1,2,3 \tag{2}$$

where K_{ij} is the porous media hydraulic conductivity tensor [L/T]; h is the freshwater head [L]; ρ_r is the relative fluid density [/]; g is the gravitational constant [L/T^2]; z is the fluid elevation [L]; ζ is the one-dimensional loading efficiency [/]; and σ_{zz} is the vertical stress [M/LT^2]. The loading efficiency is further defined as[6,7]:

$$\zeta = \frac{B(1+\nu)}{3(1-\nu) - 2\alpha B(1-2\nu)}, \quad B = \frac{\left(\frac{1}{K} - \frac{1}{K_s} \right)}{\left(\frac{1}{K} - \frac{1}{K_s} \right) + n \left(\frac{1}{K_f} - \frac{1}{K_s} \right)} \tag{3}$$

where B is the Skempton coefficient and physically represents the ratio of change in fluid pressure to a change in mean effective stress under undrained conditions.[7]

3 SUB-REGIONAL MODEL

Both steady-state and pseudo steady-state simulations need to be run prior to paleoclimate simulations. For a given modelling scenario, a steady-state simulation without total dissolved solids (TDS) is run using FRAC3DVS-OPG. The resulting freshwater heads from the steady-state simulation are modified to account for the presence of high TDS, where the development of the initial TDS distribution is described in §3.2. The adjusted freshwater heads and initial TDS distribution form the initial conditions for a 1 Ma transient simulation, whose final state at 1 Ma represents a pseudo steady-state. The resulting pseudo steady-state freshwater heads and TDS distribution are used as the initial conditions for the paleoclimate simulations.

3.1 Spatial Discretization

The three-dimensional sub-regional domain was discretized into 847 080 nodes, and 789 887 brick elements, covering an area of 104 km^2. The grid is orthogonal with each equivalent porous medium (EPM) block having the same planimetric dimensions of 50 m by 50 m and was vertically discretized into 19 layers. The top of model layer 19 is defined by a digital elevation model (DEM) using the linear interpolation method within the Spatial Analyst package of ArcView 3.2a. Layers 1 through 14 inclusive have a constant thickness, while Layers 15 through 19 have a variable thickness which depends on the elevation of surface topography.

3.2 Initial Conditions

The paleoclimate simulations require coupled density-dependent flow and transport due to the high TDS concentrations found deep in the Canadian Shield. An initial TDS distribution is required for the pseudo steady-state model. An equation for TDS versus depth d for groundwaters from the Canadian Shield, based on Figure 2b in Frape and Fritz[9], is presented as Equation (4) where TDS is in units of g/L.

$$TDS = \begin{cases} 10^{0.001981697d}, & \text{for } d \leq 1250\,\text{m}; \\ 300, & \text{for } d > 1250\,\text{m}. \end{cases} \tag{4}$$

Setting an upper bound for the TDS distribution as an initial condition allows recharge waters to reduce the TDS concentrations in fractures, and in the nearby rock matrix during the pseudo steady-state simulations, providing a more representative initial condition for the paleoclimate simulations.

3.3 Boundary Conditions

For the steady-state and pseudo steady-state models, specified head is applied to surface nodes associated with water features, while a recharge rate of 1.0 mm/a is applied elsewhere

across the top of the model. A zero-flux boundary condition for flow is applied to the model's sides and bottom. For the paleoclimate simulations, a tracer associated with water entering the groundwater model from the top surface is used to investigate glacial meltwater migration in the subsurface during and subsequent to a glaciation and deglaciation episode. A Cauchy boundary condition at the model's top surface is used with a tracer concentration of unity.

A plot of various NN2778 Glacial Systems Model (GSM) model outputs, including ice thickness and permafrost depth, for the grid cell containing the sub-regional modelling domain are shown in Figure 1. The ice thickness, lake depth, and permafrost depth outputs are applied to the paleoclimate groundwater flow simulations.

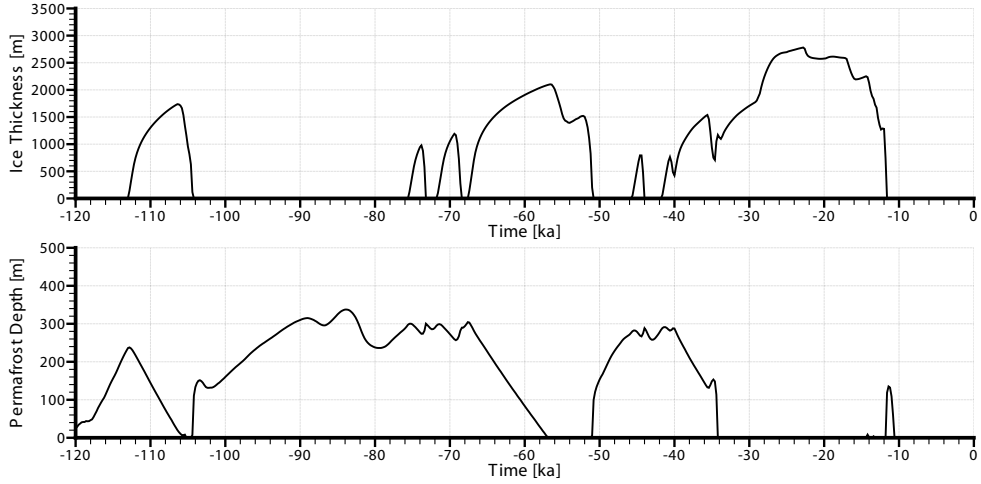

Figure 1: Plots of ice thickness and permafrost depth versus time for the nn2778 GSM grid block containing the sub-regional modelling domain, provided by Peltier [10]

3.4 Fracture Network Model

Srivastava [11] developed a framework for generating equally likely fracture network models. The first unconditioned fracture network model (FNM) from Srivastava [12] was chosen for all paleoclimate simulations. The FNM was then mapped onto an orthogonal brick element mesh whereby planar quadrilateral elements are used to represent fracture zones of higher permeability. The resulting orthogonal FNM is shown in Figure 2.

3.5 Properties

Properties for the paleoclimate simulations are provided in Table 1. The values for Young's Modulus E and Poisson's ratio ν are provided in Chan and Stanchell [13]. The calculation of specific storage S_s and one-dimensional loading efficiency ζ assume the Biot coefficient $\alpha = 0.73$ [13], and a fluid compressibility of $4.4\times10^{-10}\,\mathrm{Pa}^{-1}$. Fracture properties for solute transport include a longitudinal dispersivity of 250 m, and a transverse dispersivity of 25 m. Dispersivities

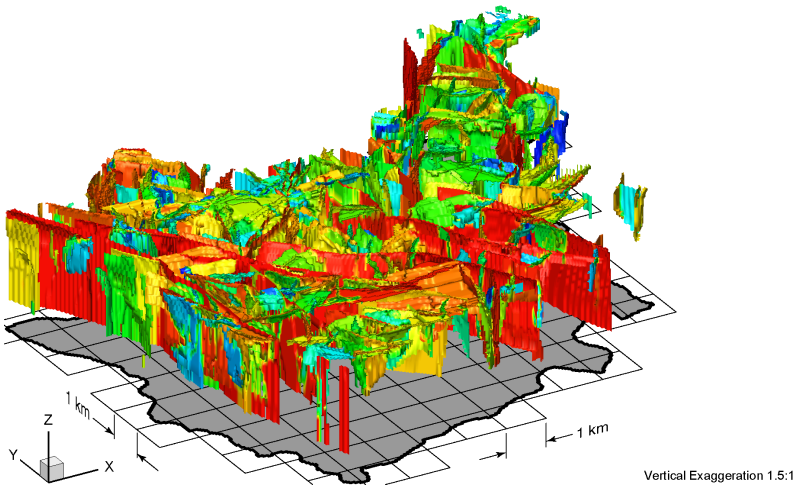

Figure 2: 3-D perspective view of orthogonal FNM

for the matrix include a longitudinal dispersivity of 50 m, a transverse horizontal dispersivity of 5 m and a transverse vertical dispersivity of 0.5 m.

Fracture zone hydraulic conductivity decreases with depth from a value of approximately 1×10^{-13} m/s at surface to 1×10^{-16} m/s at depths of 1500 m. The permafrost depths were used to select any FRAC3DVS-OPG grid block whose top face was within the permafrost zone for each time step. A permafrost hydraulic conductivity of 5×10^{-11} m/s was applied and assumed to be valid for fractured rock systems, even though McCauley et al.[14] performed experiments with frozen soils. Any fracture which is adjacent to a hexahedral element whose permeability has been reduced due to the presence of permafrost, is itself subject to the same permeability reduction.

4 PALEOCLIMATE SIMULATIONS

A steady-state simulation was performed, followed by a pseudo steady-state density-dependent simulation which was used as the initial conditions for the paleoclimate simulations. The purpose of pseudo steady-state density-dependent simulations is to allow the flow system to equilibrate from the initial TDS distribution. Solute free recharge water tends to flush fracture zones and reduce TDS in the adjacent matrix blocks.

The first paleoclimate simulation uses the parameters listed in Table 1, and represents the base-case analysis. Scenario 1 uses the NN2778 glaciation scenario, with decreasing fracture zone permeability with depth, a computed one-dimensional loading efficiency, and coupled density-dependent flow and transport. Scenario 2 is identical to Scenario 1, but applies a one-dimensional loading efficiency $\zeta = 0$ to determine the sensitivity of glacial water infiltration to the loading efficiency term in the groundwater flow equation.

Layer	Depth Range [m]	k_H [m^2]	k_V [m^2]	n [/]	TDS [g/L]	ρ [kg/m^3]	E [GPa]	ν [/]	S_s [m^{-1}]	ζ [/]
19	0–10	1.0×10^{-13}	1.0×10^{-12}	0.003	1.02	1000.7	20.0	0.25	3.76×10^{-7}	0.80
18	10–30	1.0×10^{-14}	1.0×10^{-13}	0.003	1.10	1000.7	20.0	0.25	3.76×10^{-7}	0.80
17	30–70	9.5×10^{-16}	9.5×10^{-15}	0.003	1.26	1000.8	20.0	0.25	3.76×10^{-7}	0.80
16	70–150	2.7×10^{-16}	2.7×10^{-15}	0.003	1.68	1001.1	20.0	0.25	3.76×10^{-7}	0.80
15	150–250	5.6×10^{-17}	5.6×10^{-16}	0.003	2.56	1001.7	30.0	0.25	2.55×10^{-7}	0.78
14	250–350	1.4×10^{-17}	1.4×10^{-16}	0.003	4.03	1002.7	30.0	0.25	2.56×10^{-7}	0.78
13	350–450	4.7×10^{-18}	4.7×10^{-18}	0.003	6.37	1004.2	60.0	0.25	1.34×10^{-7}	0.75
12	450–550	2.0×10^{-18}	2.0×10^{-18}	0.003	10.05	1006.7	60.0	0.25	1.35×10^{-7}	0.75
11	550–625	1.1×10^{-18}	1.1×10^{-18}	0.003	14.81	1009.9	60.0	0.25	1.35×10^{-7}	0.75
10	625–675	8.0×10^{-19}	8.0×10^{-19}	0.003	19.54	1013.0	60.0	0.25	1.36×10^{-7}	0.75
9	675–725	6.3×10^{-19}	6.3×10^{-19}	0.003	24.55	1016.4	60.0	0.25	1.36×10^{-7}	0.75
8	725–775	5.1×10^{-19}	5.1×10^{-19}	0.003	30.84	1020.6	60.0	0.25	1.37×10^{-7}	0.75
7	775–825	4.2×10^{-19}	4.2×10^{-19}	0.003	38.74	1025.8	60.0	0.25	1.37×10^{-7}	0.75
6	825–875	3.6×10^{-19}	3.6×10^{-19}	0.003	48.67	1032.4	60.0	0.25	1.38×10^{-7}	0.75
5	875–950	3.0×10^{-19}	3.0×10^{-19}	0.003	65.26	1043.5	60.0	0.25	1.40×10^{-7}	0.75
4	950–1050	2.4×10^{-19}	2.4×10^{-19}	0.003	98.38	1065.6	60.0	0.25	1.43×10^{-7}	0.75
3	1050–1200	1.9×10^{-19}	1.9×10^{-19}	0.003	179.62	1119.7	60.0	0.25	1.50×10^{-7}	0.75
2	1200–1400	1.5×10^{-19}	1.5×10^{-19}	0.003	269.40	1179.6	60.0	0.25	1.58×10^{-7}	0.75
1	1400–1600	1.3×10^{-19}	1.3×10^{-19}	0.003	300.00	1200.0	60.0	0.25	1.61×10^{-7}	0.75

Table 1: Sub-regional model properties for paleoclimate simulations with density-dependent coupling

4.1 Simulation Results

A tracer of unit concentration is applied as a Cauchy boundary condition to all inflow surface nodes at the beginning of the paleoclimate simulation. This tracer is used to characterize the migration, from the surface, of recharge water that occurs during the paleoclimate simulation; the recharge water includes glacial meltwater. The depth of glacial meltwater penetration into the subsurface is of interest because dissolved oxygen (O_2) can be transported to great depths by infiltrating meltwater, and is a consideration in repository siting. Tracer concentrations for the modelling domain are presented in Figure 3 at the end of the 120 ka simulation; the tracer is predominantly in the matrix with some tracer appearing in fractures at mid-depth.

Scenario 2 investigates the role of hydromechanical coupling, by setting the one-dimensional loading efficiency, $\zeta = 0$. The tracer, as shown in Figure 4, has migrated deeper into the subsurface as compared to Scenario 1, due to the increased vertical gradients resulting from ignoring hydromechanical coupling.

The differences between Figure 3 and Figure 4 demonstrate that hydromechanical coupling is an important process that must be considered during long-term groundwater simulations under paleoclimate conditions.

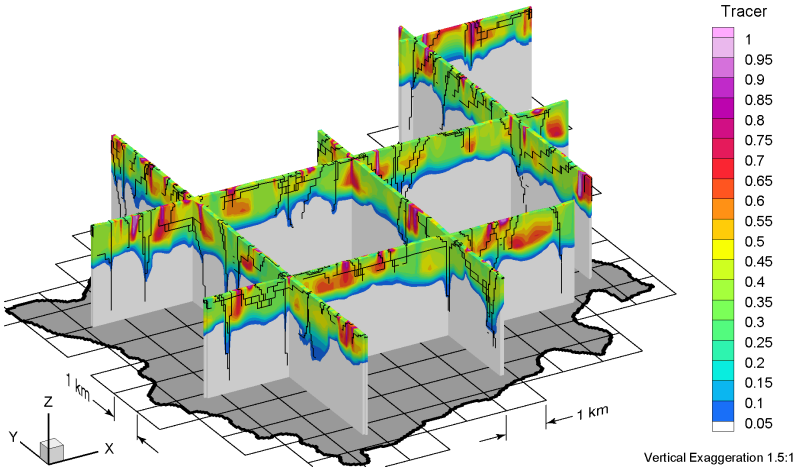

Figure 3: Migration of unit tracer during 120 ka paleoclimate simulation for computed one-dimensional loading efficiency

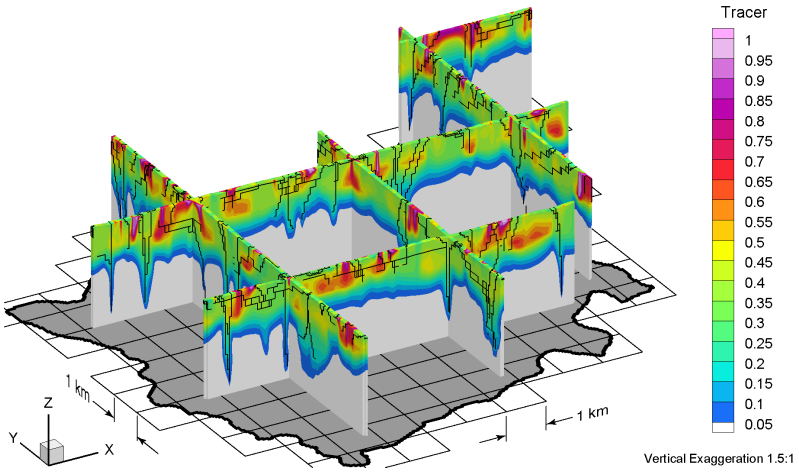

Figure 4: Migration of unit tracer during 120 ka paleoclimate simulation for one-dimensional loading efficiency $\zeta = 0$

5 SUMMARY AND CONCLUSIONS

The choice of hydromechanical coupling has significant influences on unit tracer migration. The unit tracer migrates deeper into the subsurface when ignoring hydromechanical coupling while assuming the hydraulic boundary condition at ground surface is equal to the pressure at the base of an ice-sheet. Hydromechanical coupling is a very important mechanism which affects hydraulic gradients during a glaciation event. Groundwater flow models which do not include a suitable form of hydromechanical coupling, one-dimensional or otherwise, must be used with caution as very large vertical gradients can be generated, resulting in higher pore water velocities, and enhanced migration of surface waters into the subsurface environment.

REFERENCES

[1] W.R. Peltier. A design basis glacier scenario, Technical Report 06819-REP-01200-10069-R00, Ontario Power Generation, Nuclear Waste Management Division, Toronto, Canada, (2002).

[2] A.M. Provost, C.I. Voss, and C.E. Neuzil. Site-94 – Glaciation and regional ground-water flow in the Fennoscandian Shield, SKI Report 96:11, SKI (Swedish Nuclear Power Inspectorate), Stockholm, Sweden, (1998).

[3] G.S. Boulton, U. Kautsky, L. Morén, and T. Wallroth. Impact of long-term climate change on a deep geological repository for spent nuclear fuel, Technical Report TR-99-05, SKB, Stockholm, Sweden, (2001).

[4] J. Cedercreutz. Future climate scenarios for Olkiluoto with emphasis on permafrost, Technical Report 2004-06, Posiva Oy, Olkiluoto, Finland, (2004).

[5] S.J. Marshall, L. Tarasov, G.K.C. Clarke, and W.R. Peltier. Glaciological reconstruction of the Laurentide ice sheet: Physical processes and modelling challenges. *Canadian Journal of Earth Sciences*, **37**(5), 769–793, (2000), doi:10.1139/cjes-37-5-769.

[6] G. van der Kamp and J.E. Gale. Theory of Earth tide and barometric effects in porous formations with compressible grains. *Water Resources Research*, **19**(2), 538–544, (1983), doi:10.1029/WR019i002p00538.

[7] C.E. Neuzil. Hydromechanical coupling in geologic processes. *Hydrogeology Journal*, **11**(1), 41–83, (2003), doi:10.1007/s10040-002-0230-8.

[8] J.C. Jaeger, N.G.W. Cook, and R.W. Zimmerman. *Fundamentals of Rock Mechanics*, Blackwell Publishing Ltd, fourth edition, (2007).

[9] S.K. Frape and P. Fritz. Geochemical trends for groundwaters from the Canadian Shield, in P. Fritz and S.K. Frape (Eds.), *Saline Water and Gases in Crystalline Rocks*, (1987), number 33 in Geological Association of Canada Special Paper, 19–38.

[10] W.R. Peltier. Boundary conditions data sets for spent fuel repository performance assessment, Technical Report 06819-REP-01200-10154-R00, Ontario Power Generation, Nuclear Waste Management Division, Toronto, Canada, (2006).

[11] R.M. Srivastava. The discrete fracture network model in the local scale flow system for the Third Case Study, Technical Report 06819-REP-01300-10061-R00, Ontario Power Generation, Nuclear Waste Management Division, Toronto, Canada, (2002).

[12] R.M. Srivastava. Site2a fracture network models, Compact Disc, (2005).

[13] T. Chan and F.W. Stanchell. DECOVALEX-THMC project: Task E – implications of glaciation and coupled thermohydromechanical processes on Shield flow system evolution and performance assessment, final report, SKI Report 2008:46, SKI (Swedish Nuclear Power Inspectorate), Stockholm, Sweden, (2008).

[14] C.A. McCauley, D.M. White, M.R. Lilly, and D.M. Nyman. A comparison of hydraulic conductivities, permeabilities and infiltration rates in frozen and unfrozen soils. *Cold Regions Science and Technology*, **34**(2), 117–125, (2002), doi:10.1016/S0165-232X(01)00064-7.